Applied Catalysis B: Environmental 111–112 (2012) 1–9

Contents lists available at SciVerse ScienceDirect

Applied Catalysis B: Environmental

journal homepage: www.elsevier.com/locate/apcatb

Gas-phase photocatalytic activity of nanostructured titanium dioxide from flame aerosol synthesis

Svetlana Jõks[a], Deniss Klauson[a], Marina Krichevskaya[a,*], Sergei Preis[b], Fei Qi[c], Alfred Weber[c], Anna Moiseev[d], Joachim Deubener[d]

[a] Department of Chemical Engineering, Tallinn University of Technology, Ehitajate tee 5, 19086 Tallinn, Estonia
[b] LUT Chemistry, Lappeenranta University of Technology, P.O. Box 20, 53851 Lappeenranta, Finland
[c] Institute of Particle Technology, TU Clausthal, Leibnizstrasse 19, 38678, Clausthal-Zellerfeld, Germany
[d] Institute of Non-Metallic Materials, TU Clausthal, Zehntnerstrasse 2a, 38678, Clausthal-Zellerfeld, Germany

ARTICLE INFO

Article history:
Received 10 June 2011
Received in revised form 5 September 2011
Accepted 9 September 2011
Available online 16 September 2011

Dedicated to Ass. Prof. em. Dr. Eduard Tearo and Ass. Prof. em. Dr. Endel Uus.

Keywords:
Flame aerosol synthesis
Photocatalytic activity
Titanium dioxide
Air pollution
Volatile organic compounds

ABSTRACT

The experimental evaluation of gas-phase photocatalytic activity of a TiO_2 nanopowder synthesized in a flame aerosol reactor was carried out in photocatalytic oxidation (PCO) of volatile organic compounds (VOCs). The nanopowder has an average particle size of 13 nm, anatase content 97 wt.% and the specific surface area of 102 $m^2 g^{-1}$. The performance was compared to the benchmark photocatalyst, the commercial pyrogenic titania P25, Evonik, with the average particle size of 21 nm. The full-factorial experiments were carried out varying contact times, concentrations of pollutants and temperatures in continuous gas-flow mode degrading aliphatic acrylonitrile (AN) and aromatic toluene. Higher conversions at more stable performance were observed for the flame aerosol synthesized photocatalyst in degradation of both pollutants. While the primary particle size and specific surface area present the apparent reasons for improved PCO performance in adsorbable AN, these parameters cannot do the same in oxidation of poorly adsorbable toluene: the superior generation of hydroxyl radicals and, therefore, advanced oxidative activity are proposed as explanation. The intense dehydration of reduced size anatase crystallites at elevated temperature (130 °C) presumably resulted in decreased OH-radicals production along with the improved desorption of HCN, the PCO by-product of AN. The safe performance is thus requiring lower operational temperatures. Slower deactivation and faster restoration of catalytic activity of flame aerosol synthesized catalyst under UV-A-radiation are discussed.

© 2011 Elsevier B.V. All rights reserved.

1. Introduction

Volatile organic compounds (VOCs) are common air pollutants emitted by chemical, petrochemical, pharmaceutical, and food processing industries, pulp and paper mills, and printing and painting works [1]. VOCs catalytic control technologies could be classified dependently on the pollutants' concentration levels and contaminated air flow rates [2]. Catalytic incineration and combustion techniques require as high as hundreds of ppm concentrations of VOCs and high temperatures (250–1200 °C) for successful operation being cost-ineffective for low pollutant concentrations [3–5]. Low concentrations of VOCs are mostly treated by adsorption and biological oxidation, as well as by non-thermal plasma [2,6]. Photocatalytic oxidation (PCO) technique is of extensive interest recently as potential air-cleaning technology for lower VOCs concentrations and indoor applications [7]. PCO usually uses a near UV-irradiated TiO_2 semiconductor catalyst: the method has oxidation potential sufficient to oxidize the widest spectrum of pollutants at near-ambient temperature [8–10], and is also capable of microbial contamination control of indoor air [11,12]. However, the efficiency of PCO in pollution abatement seems to depend on the chemical nature of the pollutant molecule [13]: catalyst deactivation by oxidation products is the main problem in PCO of, for example, aromatic compounds, trichloroethylene, sulphur- and silicon-containing compounds and others [14–16].Commercial pyrogenic titanium dioxide P25 (Evonik) formed in oxy-hydrogen flame is routinely used as a benchmark photocatalyst in oxidation of VOCs due to its unselective fairly good photoactivity towards wide spectra of pollutants, commercial availability and low cost. However, since the PCO of many organic vapours on P25 is not sufficiently fast for commercial process implementation and the photocatalyst is often deactivated, more active catalysts should be developed. Among various methods, the flame aerosol synthesis of nanopowders is favourable technique for controlling

* Corresponding author. Tel.: +372 6202850; fax: +372 6202856.
E-mail addresses: lanka@starline.ee (S. Jõks), deniss.klauson@ttu.ee (D. Klauson), marina.kritsevskaja@ttu.ee (M. Krichevskaya), sergei.preis@lut.fi (S. Preis), fei.qi@mvt.tu-clausthal.de (F. Qi), weber@mvt.tu-clausthal.de (A. Weber), anna.moiseev@tu-clausthal.de (A. Moiseev), joachim.deubener@tu-clausthal.de (J. Deubener).

0926-3373/$ – see front matter © 2011 Elsevier B.V. All rights reserved.
doi:10.1016/j.apcatb.2011.09.007

crystal structure, particle size and its distribution, thus resulting in generation of open-structure agglomerates [17–21] with catalytic performance exceeding commercial photocatalyst P25 in degradation of aliphatic dichloroacetic acid (DCA) and aromatic 4-chlorophenol (4-CP) in aqueous solutions [22]. The size and crystal phase composition of TiO_2 nanoparticles have been shown crucial for their activity in aqueous phase [23]. However, the lower hydration of catalyst surface in gas-phase PCO brings forward the process sensitivity to the pollutants adsorption–desorption and surface characteristics inducing the difference in photocatalytic activity with aqueous phase. The data on the efficiency of flame synthesized TiO_2 catalysts in air treatment, however, are scarce, only the degradation of acetaldehyde and methanol in batch reactor was described by Balázs et al. [24] using relatively coarse (over 50 nm) anatase nanoparticles from flame synthesis. The improved PCO efficiency in aqueous phenol removal was attributed to the increase in the polyhedral-to-spherical particles ratio, although no improvement was seen in VOCs oxidation in air. To assure the photocatalytic activity of the newly synthesized material exceeding the one of commercially available materials, the gas-phase tests are necessary.

The continuous gas-flow mode used in present research allows following the adsorption/desorption equilibrium of initial pollutants and PCO products, as well as higher concentrations of pollutants could ascertain the deactivation limits of tested photocatalytic materials. Hazardous air pollutants aromatic hydrophobic toluene and aliphatic heteroatomic acrylonitrile (AN) were chosen for gas-phase performance studies of one of the photocatalyst samples F3 synthesized by Moiseev et al. [22] in comparison with commercial P25. AN is detected as an in-door air component emitted by commercial fibrous polymeric materials, resins and smoking tobacco [25,26]; it can induce gene mutations, chromosome aberrations, unscheduled DNA synthesis and cell transformation [27]. Toluene is used as admixture to motor fuel improving octane ratings and also in the synthesis of various organic chemicals and pharmaceuticals, in the production of polymers and as a solvent in paints, coatings, synthetic fragrances, adhesives, inks and cleaning agents [28]. The central nervous system, kidneys, liver and heart are the primary targets for toluene toxicity [29].

The PCO of toluene using commercial TiO_2 catalysts has been extensively studied [30–32]. Regardless of some discrepancies in the PCO products composition, benzoic acid and benzaldehyde intermediates were found to be the products deactivating the photocatalyst [33–35]. Thus, the rate-limiting stage for toluene complete oxidation is PCO of adsorbed intermediates, the degradation rates of which are slower than the one of the parent compound [14,36]. Toluene presents serious problem in the long-term photocatalyst activity exhibiting pronounced deactivation properties [7,37]. The abundance in published data allows toluene being a reference pollutant in characterization of the catalysts and the abatement methods in general. PCO of AN vapours was less studied, the results of P25 and sulphated TiO_2 application were described in recent publications [38,39].

The objective of present paper was to evaluate the gas-phase photocatalytic activity of the new flame synthesized F3 nanopowder photocatalyst compared to commercial P25: the experiments were carried out varying the pollutant concentration, residence time and temperature following the deactivation issues.

2. Experimental

2.1. Materials and analyses

Acrylonitrile (purity ≥ 99.5%, Sigma–Aldrich) and toluene (purity ≥ 99.5%, Lach-Ner) were used as the test air pollutants.

Pyrogenic photocatalyst Aeroxide TiO_2 P25 from Aerosil® process was kindly donated by Evonik Industries (Hanau, Germany) [40–42]. The photocatalyst material labelled F3 used in this study was synthesized as described in [22]: the vapour of the catalyst precursor titanium tetrachloride was formed by passing dry argon gas through a bubbler submerged to the $TiCl_4$-liquid at room temperature. Methane, oxygen and nitrogen were premixed with Ar/$TiCl_4$ and the mixture was introduced into the burner. The flame temperature during synthesis was about 900 °C. The TiO_2 particles were collected on a glass fibre filter placed about 50 cm above the flame. The overall synthesis reaction is given in Eq. (1):

$$TiCl_4(g) + 4O_2(g) + 2CH_4(g) \rightarrow TiO_2(s) + 4HCl(g) + 2CO_2(g) + 2H_2O(g) \quad (1)$$

The feed flow rate of Ar/$TiCl_4$ was varied between 5 and 60 L h^{-1} with the synthesized TiO_2 samples labelled from F1 to F6 in ascendant row of manufacturing rate. The PCO activity of the photocatalyst materials was studied with the aqueous solutions of DCA and 4-CP (see Section 1) ranking the materials in the ascendant order: P25 < F6 < F5 < F4 < **F3** ≅ F1 ≅ F2 [22]. F3 produced at 12 L h^{-1} of Ar/$TiCl_4$ feed rate was selected for gas-phase PCO study as the one with high photocatalytic activity.

The specific surface area of titania powders was determined from the five-point nitrogen adsorption isotherm obtained from Brunauer–Emmett–Teller (BET) measurements using the Gemini 2360 Surface Area Analyzer (Micromeritics, USA). Transmission electron microscopy (TEM) micrographs were obtained with the JEM-2100 microscope (JEOL) operating at 120 kV. The average primary particle size d_{TEM} was estimated as of more than 300 particles. The crystalline phase composition was analysed by X-ray diffraction (XRD) using a Siemens D5000 Kristalloflex instrument and scanning the 2θ range from 15 to 70° at the increment of 0.04°. The relative weight fraction of rutile was determined using Rietveld full-profile refinement with Topas R Software.

Diffuse reflection spectra of P25 and F3 were obtained on a UV-Vis-NIR spectrophotometer Perkin-Elmer Lambda 950, equipped with 150 mm integrating sphere, using Spectralon® as white reference. Simultaneous thermal gravimetric (TG) and differential thermal gravimetric (DTG) analyses were performed on Netsch STA 409 PC Luxx thermal analyzer (TG resolution 2 μg) coupled with mass spectrometer (MS) gas analysis system QMS 403C Aeolos; 100 mg of photocatalyst material was heated in Al_2O_3 crucible with a heating rate of 10 K min^{-1} under nitrogen gas conditions (flow rate of 1 mL min^{-1}).

2.2. Preparation of TiO_2 coating

For photocatalytic experiments the photocatalyst material was fixed to the inner walls of the reactor; the surface of the lamp was free from the catalyst. The coating was formed by the 10-wt.% TiO_2 slurry in distilled water mechanically stirred overnight. The reactor vessel was repeatedly rinsed with TiO_2 slurry with each rinse followed by drying at 120 °C for 2 h. The weighted TiO_2 coating mass of 0.9 g corresponded to the catalyst loading of 1.2 mg TiO_2 per cm^2 of irradiated reactor surface. The roughness of both suspension coatings measured by means of surface profiler TENCOR P-10 was in the range of 1 μm.

Field emission scanning electron microscopy (FE SEM, Dual-Beam Helios Nanolab 600, FEI) was performed to visualize the catalyst coating.

2.3. Photocatalytic tests

Gas-phase photocatalytic experimental equipment was described in detail by Krichevskaya and Preis [36]. The

experimental equipment consists of a thermostatted reactor, gas flow controllers and INTERSPEC 200-X FTIR spectrometer with the Specac Tornado 8-m 1.33-L gas cell with ZnSe-windows. Annular lamp-in-pipe borosilicate glass reactor with total volume of 0.191 L was operated in continuous gas-flow mode. The reactor was composed of an inner glass tube (35 mm outer diameter) and an outer glass tube (45 mm inner diameter, 305 mm length).

A 15 W fluorescent lamp (Philips) with UV-A intensity of 5 mW cm^{-2} was positioned coaxially in the reactor. The UV-A irradiance passing the TiO_2-coating to the reactor's annular clearance space was measured with the UVX Radiometer (Micropulse Technology) and averaged 0.46 for the F3 and 0.15 mW cm^{-2} for P25. No UV-A radiation was detected outside the reactor, *i.e.* no UV-A radiation passed through the double coating of titania.

The VOC feed tank was charged with polluted air by tank evacuation and injection of appropriate model pollutant through the injection port. After 15 min of evaporation, the tank was pressurised with compressed air to 3 bar and left for the concentration balancing overnight. The polluted air stream was diluted with the carrier gas, dry air. The gas flow controllers provided gas flow rates from 0.5 to 4.0 L min^{-1} resulting in pollutant residence time in the reactor from 3 to 23 s. The runs lasted for 60 min with the continuous FT-IR outlet gas analysis.

The temperature in the reactor was maintained at 60 or 130 °C controlled by the heat of the lamp, reactor's insulation and heating tape with the temperature controller (Omega CN9000A).

At the end of each run, the photoreactor with UV lamp and air flow remained turned on was heated up to 180 °C for 3 h after the experiments with AN and for 15 h with toluene to restore the photocatalyst activity. The catalyst's dark adsorption and reproducible PCO activity in subsequently repeated experimental runs were considered as criteria of the catalysts restoration, which practically coincided with the restored white colour of photocatalysts.

Photocatalytic reaction of acrylonitrile and toluene was studied in pollutants' concentration range from 10 to 100 ppm. The AN peaks at the IR bands from 840 to 1100 cm^{-1} and toluene peaks at the IR bands from 700 to 750 and from 2850 to 3130 cm^{-1} were quantified with the detection limit of 1 ppm. The AN and toluene PCO gas-phase products, *i.e.* nitrogen and carbon oxides, water and hydrogen cyanide, were monitored qualitatively and their amounts were relatively compared in arbitrary units by means of FT-IR outlet gas analysis.

Table 1
Characteristics of TiO_2 powders.

TiO_2	BET, $m^2\ g^{-1}$	Average particle size d_{BET}, nm	Average particle size d_{TEM}, nm	Rutile fraction, wt.%
P25	52	29	21	13
F3	102	15	13	3.4

3. Results

3.1. Characterization of photocatalytic materials and coatings

The characteristics of both powders are shown in Table 1. Primary particles of P25 and F3 powders and their agglomerates are shown in Fig. 1.

The morphology of flame aerosol synthesised F3 is similar to that of the commercial product P25: the individual titania particles are linked together in chains forming agglomerates of a few hundred nanometres. The primary particles of both materials are of cubic or polyhedral structure. The calculated average particle size of F3, however, is considerably smaller than that of P25 with d_{TEM} of 13 nm and 21 nm respectively. The flame synthesised titania is as a rule non-porous [20,21]: the d_{BET} (15 nm) of F3 is in good agreement with d_{TEM} (13 nm), whereas d_{BET} of P25 (29 nm) is considerably bigger than d_{TEM} (21 nm) due to higher degree of agglomeration of commercial product.

The primary particle size distributions and diffuse reflectance spectra of P25 and F3 photocatalysts are compared in Fig. 2. The primary particle size distributions of both materials, as determined

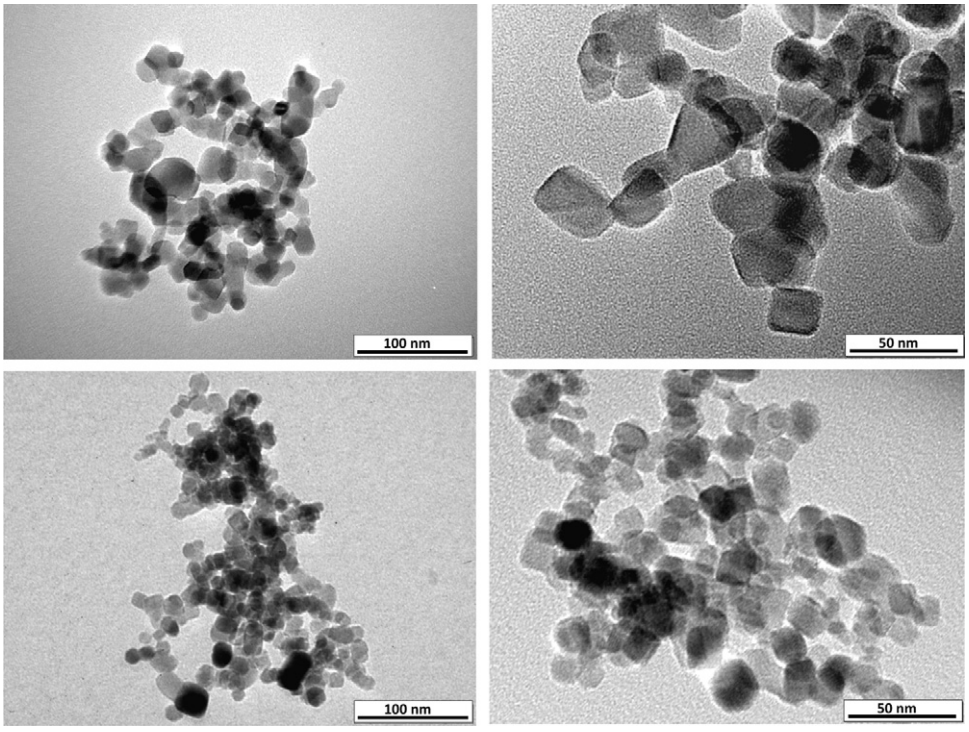

Fig. 1. TEM-images of pyrogenic TiO_2 powders: P25, upper; F3, lower.

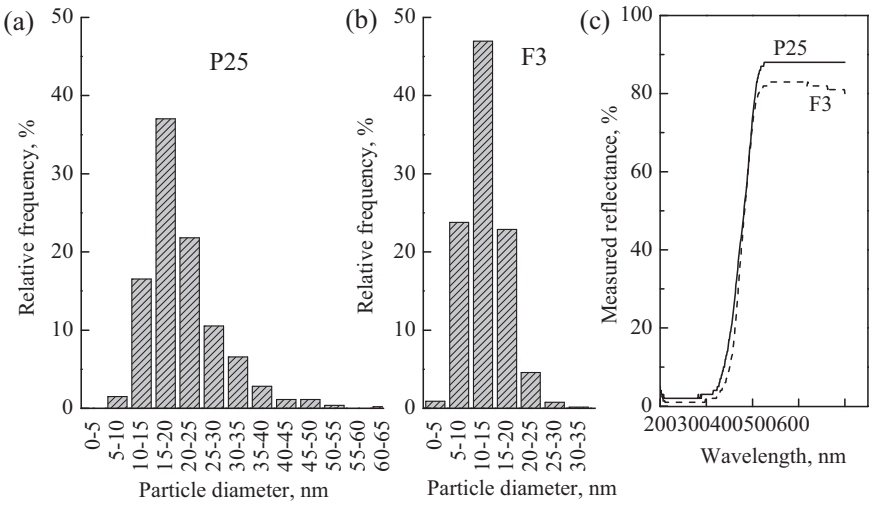

Fig. 2. Primary particle size distribution (a and b) and reflectance spectra (c) of P25 and F3 powders.

from TEM micrographs, are monomodal with a maximum frequency value for a particle size of 15–20 nm and 10–15 nm for P25 and F3 respectively. The diffuse reflectance spectra of P25 and F3 powders have shown no discrepancies in UV-A range. The higher reflectance of P25 in the range between 400 and 600 nm is caused by its higher agglomeration degree.

Although the primary particle size of P25 averages around 21 nm, there is a substantial coarse (about 6% of 35–70 nm) fraction. The inclusions of large crystallites could be also viewed in the agglomerate photo (Fig. 1). The primary particle size distribution of F3 is narrower compared to P25 and contains noticeable fraction, about 25%, of particles sized below 10 nm. The fraction sized above 35 nm is practically absent. However, no "blue" shift in absorption edge of F3 in the range between 300 and 400 nm was observed.

The results of P25 and F3 TG analysis in conjunction with MS (Fig. 3) show the mass loss and the rate of desorption (DTG) of adsorbed water. The DTG and the mass loss were about three times higher for F3 powder at 130 °C, the highest PCO temperature studied, compared to P25, although the difference in specific surface of photocatalytic materials is about the factor of two (Table 1). The considerable water desorption started at temperatures over 50 °C and was still observed at temperatures over 200 °C. The mass loss at 222 °C (filled symbols) achieved 0.75% and 1.85% for P25 and F3 respectively. The broad and intensive peak of appropriate DTG curves (open symbols) located at approximately 100 °C was attributed by mass spectrometry to physically adsorbed water. As expected, desorption of bigger quantity of water was observed for F3 having larger surface area.

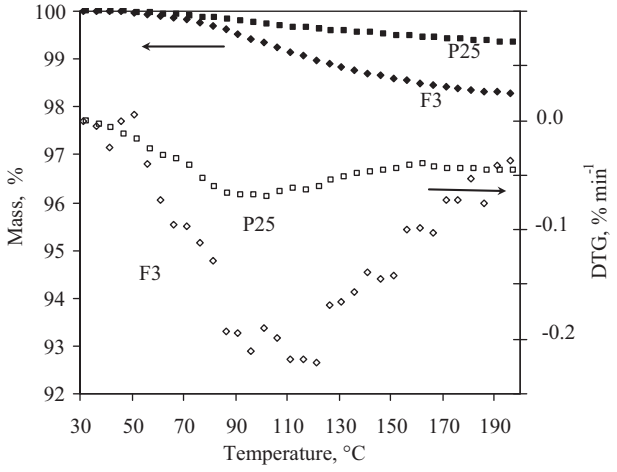

Fig. 3. Thermal analysis profiles of P25 and F3 powders: TG, filled symbols; DTG, open symbols.

The SEM images of photocatalyst coatings on borosilicate glass are given in Fig. 4. The individual nanoparticles of photocatalyst materials could be seen in the images with higher resolution. The P25 and F3 coatings show different surface topography and a smoother surface is observed with F3. The difference in agglomeration of TiO_2 particles is apparent in light transmittance through the coating: at equal catalyst coverage, 1.2 mg cm^{-2}, the F3 layer was less opaque and weakens the UV-A intensity about 11 times, whereas P25 coating makes the UV-A light weaker for about 32 times (see Section 2.3). In addition to the F3 less extensive agglomeration, the difference in coatings transparency is also attributed to the plate-like shape of F3 agglomerates different from the spherical one of P25 [22].

3.2. PCO of acrylonitrile

Acrylonitrile at its inlet concentration of 40 ppm at 60 °C and residence time of 23 s was completely adsorbed in the dark on F3 and P25 during the first 40 and 20 min respectively. The difference in adsorption was determined by smaller particles' size and larger contact surface area of F3. After 60 min of experimental run of dark adsorption the concentration of AN in the outlet gas stream comprised about 30% of the AN concentration entered the reactor for both catalysts. At 130 °C the AN adsorption showed similar tendency slightly earlier showing AN in the outlet stream at somewhat smaller adsorbed AN amounts.

The PCO of AN on F3 was examined in the full-factorial experiment at four contact times 3, 6, 11.5 and 23 s, three concentrations 10, 40 and 100 ppm, and two temperatures 60 and 130 °C. The temperature was maintained by working UV-lamp dependent on the insulation of reactor. At 130 °C some aid of the heating tape was applied.

No AN was observed in the outlet of reactor due to its adsorption and conversion ($1-(C_{out}/C_{in})$, %) at 130 °C at all residence times and AN concentrations, as well as at 60 °C at residence times from 11.5 to 23 s over both photocatalysts. The difference in P25 and F3 performance appeared only at 60 °C at residence times of 3 and 6 s with higher AN concentrations, 40 and 100 ppm. The variations in the AN conversion with the residence time of 3 s at 60 °C for both photocatalysts are shown in Fig. 5.

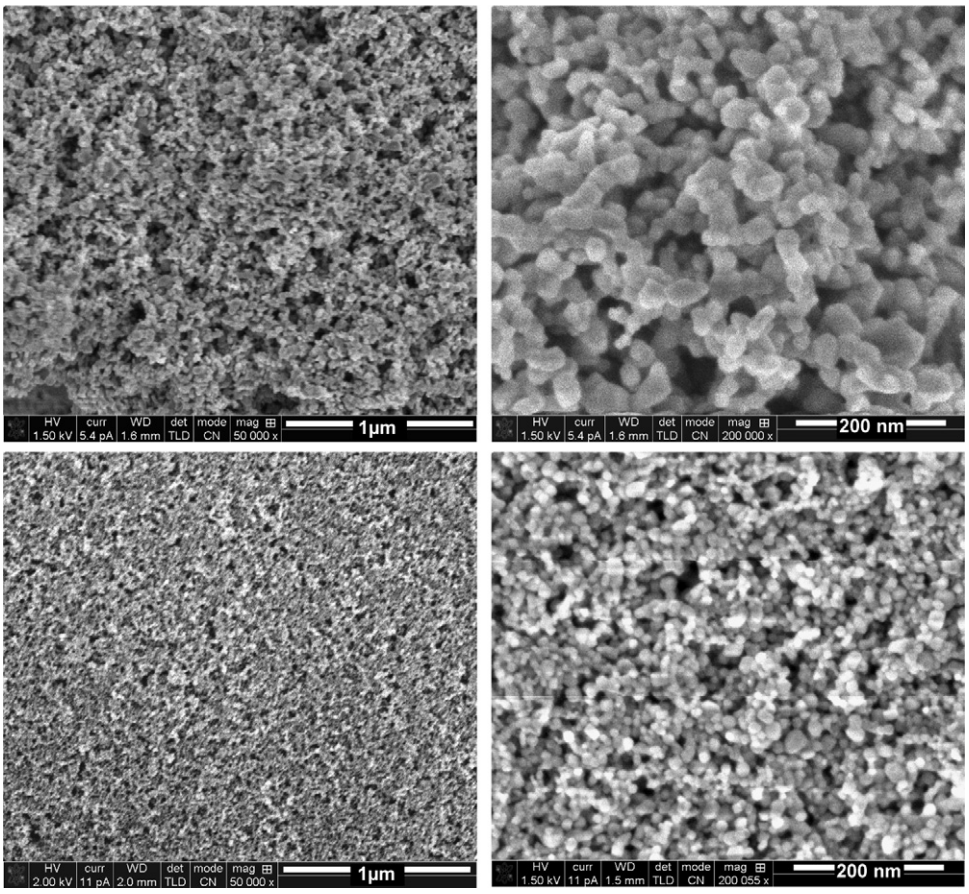

Fig. 4. SEM images of TiO_2 coatings: P25, upper; F3, lower.

From Fig. 5 one can see no AN in the outlet of reactor with F3 coating even at the shortest residence time and high concentrations of AN, whereas deterioration of P25 performance (40 ppm) and even the tendency of its deactivation (100 ppm) were observed.

Besides carbon dioxide and water, the ultimate PCO products, by-products of AN PCO include nitrous oxide, hydrogen cyanide and carbon monoxide in gaseous phase and nitric acid as the product adsorbed on the photocatalyst. The by-products of AN PCO were discussed in detail previously [38,39]. No difference in by-products composition between F3 and P25 was observed.

However, the moment of occurrence of unfavourable HCN within the experimental run time varied for the photocatalysts at 130 °C (see Fig. 6). Hydrogen cyanide did not appear immediately at the starting point of experimental runs, but did in a few minutes; the occurrence of HCN is thus concerned to accumulation of surface-adsorbed reaction products. Hydrogen cyanide was seen to oxidise further to NO_2 forming HNO_3 with water [39]. At 60 °C equal amounts of HCN appear at the same time with both photocatalysts, thus making the overall yield of gaseous hydrogen cyanide per unit of oxidised AN higher for P25, where degradation of AN is incomplete (Fig. 5).

The occurrence of hydrogen cyanide during PCO of AN on the F3 titanium dioxide coating occurred earlier than on P25 mostly at the higher temperature, shorter residence time and lower AN concentrations.

3.3. PCO of toluene

Toluene, being weakly adsorbed on TiO_2 at relatively low temperatures [43], did not adsorb on P25 at 60 and 130 °C. While no adsorption of toluene on F3 was observed at 130 °C, 40% of total toluene amount in the stream containing 40 ppm at residence time

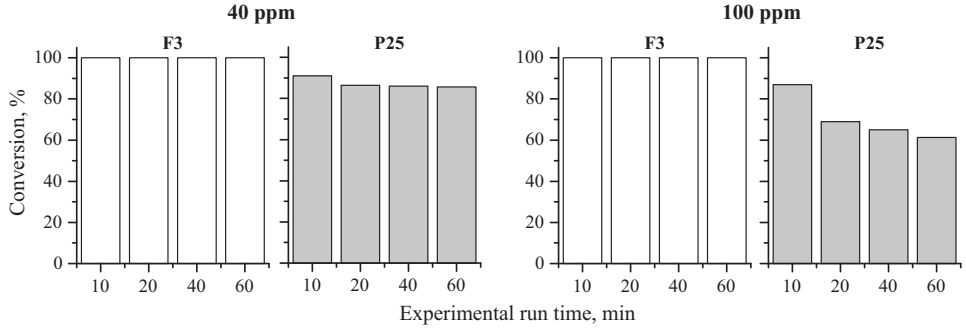

Fig. 5. Acrylonitrile PCO conversion at 60 °C and residence time of 3 s.

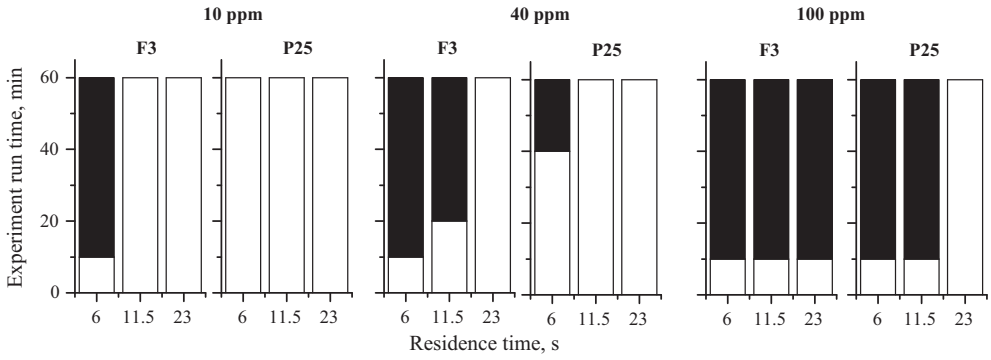

Fig. 6. The occurrence (time, min) of HCN (black columns) during the experimental run with AN at 130 °C.

of 23 s were adsorbed before reaching the adsorption equilibrium at 60 °C, indicating a potential for successful PCO of toluene on F3 photocatalyst.

In the present study toluene expectedly deactivated the photocatalysts. However, at sufficiently low concentration (10 ppm) at residence times from 6 to 23 s at both temperatures no poisoning of both photocatalysts was observed. Moreover, at the longest residence time 23 s no variations in toluene conversion within 60-min run over both catalysts were observed at the toluene initial concentration of 40 ppm at both temperatures, although slight change in photocatalyst colour from white to yellowish indicated possible catalyst deactivation in longer runs. The considerable difference in photocatalysts' performance, however, appeared at shorter residence times of 6 and 11.5 s. Noticeable deterioration in toluene conversion took place at P25 photocatalyst (Fig. 7): at the residence time of 11.5 s the toluene conversion dropped two-fold in 1 h at both temperatures, whereas F3 showed no decline in performance. The F3 photocatalyst showed noticeably slower deactivation in comparison with P25. Earlier photocatalysts deactivation at higher temperature was observed.

There was also noticeable difference in restoration of photocatalyst activity, which was faster for F3 photocatalyst: necessary treatment time to restore the photocatalyst activity and white colour was about 5 h for F3 at the highest toluene concentration and up to 15 h for P25 under identical experimental conditions. This difference could be explained by better UV-light transparency of F3 coating along with its enhanced oxidative ability.

The UV-A radiation passing the TiO_2-coating to the reactor's annular clearance space comprised 9% and 3% for F3 and P25 respectively (see Section 2.3). It could be assumed then that the amount of the UV photons is higher in the intertubular space of F3-reactor allowing its faster restoration.

4. Discussion

The following observations requiring discussion were made:

- higher conversions and stable performance of flame aerosol synthesized F3 photocatalyst towards the degradation of AN and toluene;
- slower deactivation and faster restoration of catalytic activity of F3 catalyst under UV-radiation;
- the earlier, within the experimental run time, appearance of HCN as the AN PCO by-product and, in general, poorer performance of F3 catalyst in HCN abatement at elevated temperatures.

The observations somewhat contradict each other in terms of the new catalyst characterization: the performance of flame aerosol synthesized catalyst substantially improved in toluene and AN oxidation, occurs to be accompanied with enhanced emission of undesired AN PCO by-product hydrogen cyanide, which, although noticed only at the elevated temperature and thus possibly avoided, reveals limitations earlier unknown for the photocatalysts development.

4.1. Improved photocatalytic performance

The improved F3 unselective PCO performance towards well-adsorbed AN and weakly adsorbed toluene indicates the higher oxidative ability of F3 photocatalyst, achieved due to F3 titanium dioxide particle size, increased TiO_2-surface area exposed to irradiation, structural properties and, therefore, superior oxidative ability. The superior character of flame aerosol synthesized catalyst over the benchmark P25 is thus confirmed for the gas-phase PCO similar to the observed in aqueous reactions: both well-adsorbed aliphatic DCA (aq.) and AN (gas), and weakly adsorbed 4-CP (aq.) and toluene (gas) yielded better to PCO at the flame aerosol catalyst [22].

One of the apparent reasons for the improved photocatalytic ability is the catalyst primary particle size and shape: 13 nm F3 particles at least double the surface of 21 nm P25. The positive impact of the reduced particle size is known: the undesired recombination of photogenerated charge carriers in the volume and at the surface of the particle limiting the photocatalysts' activity [44] is reduced due to the migration time of photogenerated charge carriers proportional to the square of the particle size [45]. The overall number of surface active sites also increases with decreasing particle size resulting in accelerated interfacial charge transfer and, consequently, the increased quantum yield [45,46]. Another reason may concern the increased content of anatase thus making the idea of anatase-rutile synergism in gas-phase PCO requiring more detailed quantification. The decreased particle size and the increased content of anatase, however, not always result in improved photocatalytic properties of the catalysts [47], which makes further research in the catalyst properties needed.

The primary particle size, higher anatase content and lower agglomeration degree present the apparent reasons of improved PCO performance for AN adsorbable at the catalyst's surface. The improved performance in poorly adsorbable toluene oxidation, however, cannot be solely explained by larger adsorbing surface: non-adsorbable VOCs should mostly be oxidized by surface OH-radicals, the yield of which also, but not exclusively, is dependent on the water content at the catalyst surface. The water surface content showed disproportional relation to the photocatalysts' specific surface or saturation time – two-fold increased contact surface of F3 adsorbed three-fold amount of water compared to P25 (see Fig. 3), which may also explain accelerated toluene PCO with F3 at all temperatures studied.

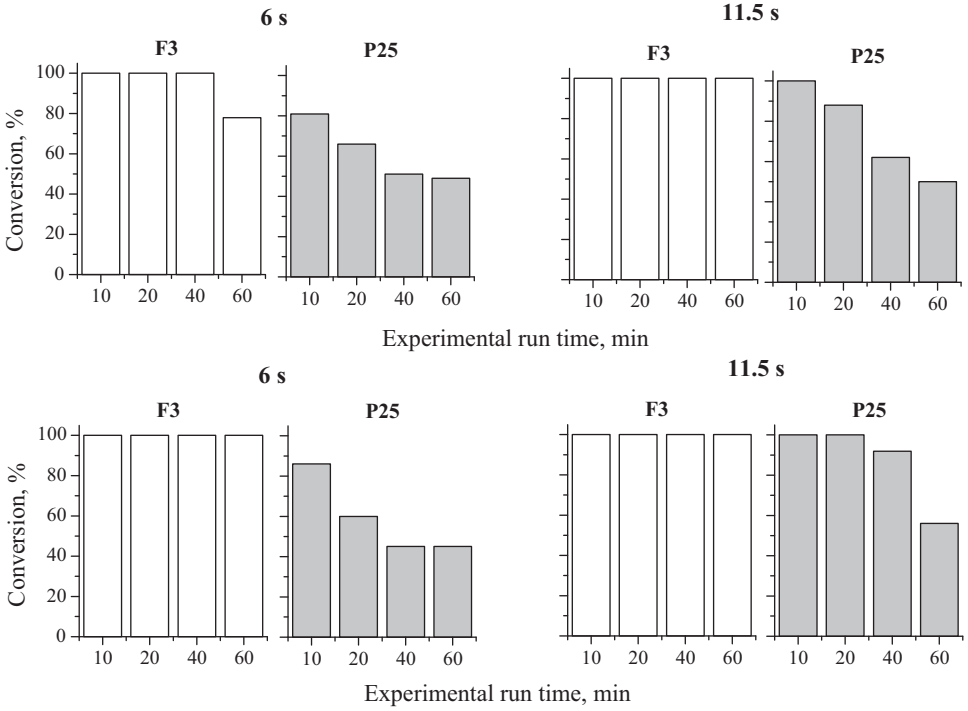

Fig. 7. Toluene PCO conversion at 130 °C (upper) and 60 °C (lower) at inlet concentration of 40 ppm and residence times of 6 and 11.5 s.

4.2. Improved stability

Although there was no decrease in toluene conversion over F3 seen at residence times of 6 and 11.5 s at 60 °C and 11.5 s at 130 °C during the 60-min experimental run, the changes in photocatalyst colour from white to different shades of yellow indicated by-products of toluene oxidation adsorbed on the photocatalyst surface tending towards the catalyst poisoning. At the shortest residence time of 6 s at 130 °C, the photocatalyst deactivation started in 1 h. This could be explained by increased accumulation of toluene PCO intermediates at higher temperatures [48]. This is in an agreement with PCO of toluene on P25, where conversion of toluene dropped from 100 to 60% in 40 min at 130 °C, while it decreased only from 100 to 90% during the same time at 60 °C. No products other than CO_2, CO and H_2O were seen also during the temperature-programmed oxidation after toluene PCO run, where the temperature was raised up to 350 °C, as the main adsorbed PCO by-products also decompose to carbon oxides and water at about this temperature [14].

The recovery of F3 carried out at 180 °C in dry air was accomplished about three times faster than of P25 also indicating stronger photocatalytic potential of the flame aerosol synthesized catalyst. The photocatalytic activity was restored entirely after each of multiple runs.

4.3. Hydrogen cyanide emission

The more incomplete hydrogen cyanide oxidation at elevated temperature with F3 compared to P25 may follow two non-contradictory explanation patterns, the dehydration of the catalyst surface resulted in reduced OH-radicals production at higher temperature (130 °C), and the HCN volatility drastically surpassing the volatility of AN.

Photocatalytic reactions usually are not sensitive to minor variations in temperatures, since the by-product desorption step determines the rate at lower temperatures, whereas the adsorption of reactants is rate determining at higher temperatures [49–51]. When two catalysts with different crystallographic composition and average particle size are compared, the difference in their activity loss at different temperatures is mostly due to their crystallites structure and surface properties. The alteration of photo-production of radicals on heated titanium dioxide was shown by Gonzalez-Elipe et al. [52] and Nakaoka and Nosaka [53]: the change in the radicals' production is caused by the desorption of surface hydroxyl groups and the consequential change in the surface structure. Different reactivity radicals are thus supposed to be formed at different temperatures. The difference in photo-produced radicals at different temperatures could cause the difference in reactivity of the crystallites towards hydrogen cyanide. Bickley and Stone [54] suggested that the loss of adsorbed water would appear to be the main factor governing the decrease in the photoactivity of TiO_2. By measuring the photoadsorption of oxygen and by the quantitative determination of OH groups on the same sample Boonstra and Mutsaers [55] were able to relate these two properties. From the linear relation of oxygen photoadsorption to number of hydroxyl groups after outgassing at different temperatures they concluded that the photoactivity of TiO_2 is determined by the TiOH groups on the surface. It was also found that anatase is more photosensitive to oxygen than rutile. It could be also supposed that anatase crystallites of different sizes possess different sensitivities towards the increased temperature differently loosing the activity due to dehydration. The activity of Pt-group catalysts is also known to be highly sensitive to their particles' size, shape and crystallographic orientation [56–58].

Aqueous photocatalytic oxidation of cyanide was studied earlier and the results may also support the explanation of HCN emission at elevated temperature. The aqueous PCO of cyanide occurs *via* a pure heterogeneous pathway involving the surface hydroxyl groups [59]. The quantum efficiency of the photocatalytic oxidation was found to be low mainly due to the poor adsorption of cyanide ions onto the titanium dioxide surface and, the most important, the absence of homogenous reaction between cyanide ions and diffused hydroxyl radicals.

Table 2
Vapour pressure of selected compounds [61,62].

Compound	Vapour pressure, kPa		
	20 °C	60 °C	130 °C
Toluene	2.9	18.5	170
AN	11.9	57	193[a]
HCN	83	356	1858

[a] At 100 °C.

The gas-phase mechanism of cyanide oxidation is not well-established yet, although the gas-phase and adsorbed products of nitrile group oxidation, N_2O and NO_2 [39], differ greatly from aqueous oxidation products, cyanate and ammonium [59]. Therefore the photocatalyst surface dehydration at 130 °C could be the factor reducing the photocatalytic activity of the catalysts towards cyanide oxidation not significantly hindering the AN oxidation.

Simultaneously, the earlier HCN occurrence on F3 at higher temperature could be attributed to its poor adsorption properties. The different morphology of catalysts result in the rate of water desorption from F3 three-fold exceeding that from P25 indicating poor retention properties of F3 at a higher temperature, also applicable to weakly adsorbed hydrogen cyanide [60]. The HCN high volatility, about six-fold higher than of AN (Table 2) [61,62], also may contribute to the HCN incomplete oxidation at 130 °C. Being extremely unwanted, hydrogen cyanide, however, is easily avoidable under properly selected experimental conditions [39].

5. Conclusions

The superior character of the flame aerosol synthesized catalyst over the commercial P25 titanium dioxide in gas-phase PCO was established for degradation of aliphatic heteroatomic acrylonitrile and aromatic toluene. This supports the unselective character of newly designed catalyst universal for both gaseous and aqueous PCO reactions. The new catalyst surpasses the commercial P25 in, for example, toluene oxidation for over 50% under similar experimental conditions. Slower deactivation and faster complete restoration of catalytic activity of flame synthesized catalyst under UV-A-radiation are also the new catalyst's beneficial key features.

Not only the primary particle size and specific surface area are the reasons for improved PCO performance: the intrinsic materials' properties, such as superior generation of hydroxyl radicals and, therefore, superior oxidative activity may explain the advanced PCO performance with non-adsorbable toluene.

The intense dehydration of the reduced size anatase crystallites in the new catalyst results in decreased OH-radicals production at elevated temperature. Along with the enhanced desorption, this causes a poorer catalyst's performance in PCO of HCN, the PCO product of acrylonitrile. The process safety thus requires lower operational temperatures.

Acknowledgements

The authors express their gratitude to the Estonian Science Foundation (grants 7541 and GUS10), Estonian project SF0140022s10, the United States Civilian Research and Development Foundation (grant ESC2-2974-TL-09) and the Deutsche Forschungsgesellschaft (DFG) (grants DE 598/16-1 and We 2331/10-1) for financial support of the research.

References

[1] R.R. Eldon, D.V.S. Murthy, T. Swaminathan, Process Biochem. 40 (2005) 2771–2779.
[2] S. Revah, J.M. Morgan-Sagastume, in: Z. Shareefdeen, A. Singh (Eds.), Biotechnology for Odor and Air Pollution Control, Springer, Berlin/Heidelberg, 2005, pp. 29–63.
[3] D.R. van der Vaart, W.M. Vatvuk, A.H. Wehe, J. Air Waste Manage. Assoc. 41 (1991) 92–98.
[4] A. Gervasini, V. Ragaini, Catal. Today 60 (2000) 129–138.
[5] W.C. Hung, H. Chu, J. Environ. Eng. 132 (2006) 1482–1488.
[6] K. Hirota, H. Sakai, M. Washio, T. Kojima, Ind. Eng. Chem. Res. 43 (2004) 1185–1191.
[7] Y. Paz, Appl. Catal. B 99 (2010) 448–460.
[8] D.M. Blake, Bibliography of Work on the Heterogeneous Photocatalytic Removal of Hazardous Compounds from Water and Air, Report, National Renewable Energy Laboratory (NREL), Golden, USA, 1995.
[9] D.T. Tompkins, Evaluation of photocatalytic air cleaning capability: a literature review and engineering analysis, ASHARE Research Project RP-1134, 2001.
[10] J. Zhao, X. Yang, Build. Environ. 38 (2003) 645–654.
[11] D.Y. Goswami, D.M. Trivedi, S.S. Block, J. Sol. Energy Eng. 119 (1997) 92–96.
[12] F. Chen, X. Yang, H.K.C. Mak, D.W.T. Chan, Build. Environ. 45 (2010) 1747–1754.
[13] A.J. Maira, K.L. Yeung, J. Soria, J.M. Coronado, C. Belver, C.Y. Lee, V. Augugliaro, Appl. Catal. B 29 (2001) 327–336.
[14] S.A. Larson, J.L. Falconer, Catal. Lett. 44 (1997) 57–65.
[15] D.F. Ollis, CR Acad. Sci. II C 3 (2000) 405–411.
[16] S.O. Hay, T.N. Obee, C. Thibaud-Erkey, Appl. Catal. B 99 (2010) 435–441.
[17] G.D. Ulrich, Chem. Eng. News 6 (1984) 22–29.
[18] S.E. Pratsinis, Prog. Energy Combust. Sci. 24 (1998) 197–219.
[19] W.J. Stark, S.E. Pratsinis, Powder Technol. 126 (2002) 103–108.
[20] R. Strobel, W.J. Stark, L. Mädler, S.E. Pratsinis, A. Baiker, J. Catal. 213 (2003) 296–304.
[21] R. Strobel, A. Baiker, S.E. Pratsinis, Adv. Powder Technol. 17 (2006) 457–480.
[22] A. Moiseev, F. Qi, J. Deubener, A. Weber, Chem. Eng. J. 170 (2011) 308–315.
[23] Z. Zhang, C.-C. Wang, R. Zakaria, J.Y. Ying, J. Phys. Chem. B 102 (1998) 10871–10878.
[24] N. Balázs, A. Gácsi, A. Pallagi, K. Mogyorósi, T. Alapi, P. Sipos, A. Dombi, React. Kinet. Mech. Catal. 102 (2011) 283–294.
[25] G. Byrd, K. Fowler, R. Hicks, M. Lovette, M. Borgerding, J. Chromatogr. A 503 (1990) 359–436.
[26] G. Scherer, J. Engl, M. Urban, G. Gilch, D. Janket, K. Riedel, Regul. Toxicol. Pharmacol. 47 (2007) 171–183.
[27] A. Léonard, G.B. Gerber, C. Stecca, J. Rueff, H. Borba, P.B. Farmer, R.J. Sram, A.J. Czeizel, I. Kalina, Mutat. Res. 436 (1999) 263–283.
[28] EPA – Environmental Protection Agency, Integrated Risk Information System (IRIS) on Toluene, National Center for Environmental Assessment, Office of Research and Development, Washington, 1999.
[29] ATSDR – Agency for Toxic Substances and Disease Registry, Toxicological Profile for Toluene, U.S. Public Health Service, U.S. Department of Health and Human Services, Atlanta, 1994.
[30] T. Ibusuki, K. Takeuchi, Atmos. Environ. 20 (1967) 1711–1715.
[31] R. Méndez-Román, N. Cardona-Martínez, Catal. Today 40 (1998) 353–365.
[32] V. Augugliaro, S. Coluccia, V. Loddo, L. Marchese, G. Martra, L. Palmisano, M. Schiavello, Appl. Catal. B 20 (1999) 15–27.
[33] E. Piera, J.A. Ayllon, X. Domenech, J. Peral, Catal. Today 76 (2002) 259–270.
[34] C. Belver, M.J. Lopez-Munoz, J.M. Coronado, J. Soria, Appl. Catal. B 46 (2003) 497–509.
[35] J. Mo, Y. Zhang, Q. Xu, J. Joaquin Lamson, R. Zhao, Atmos. Environ. 43 (2009) 2229–2246.
[36] M. Krichevskaya, S. Preis, J. Adv. Oxid. Technol. 6 (2003) 150–157.
[37] T.N. Obee, R.T. Brown, Environ. Sci. Technol. 29 (1995) 1223–1231.
[38] M. Krichevskaya, S. Jõks, A. Kachina, S. Preis, Photochem. Photobiol. Sci. 8 (2009) 600–603.
[39] S. Jõks, M. Krichevskaya, S. Preis, Catal. Lett. 141 (2011) 309–315.
[40] Titanium Dioxide P25—Manufacture—Properties—Applications, Technical Bulletin Fine Particles, Evonik Degussa Corp., Number 80, 2003.
[41] Basic Characteristics of Aerosil, Technical Bulletin Fine Particles, Evonik Degussa Corp., Number 11, 2006.
[42] C. Schulze Istfort, M. Rochnia, Toxicol. Lett. 186 (2009) 148–151.
[43] M.C. Blount, J.L. Falconer, J. Catal. 200 (2001) 21–33.
[44] C.-Y. Wang, J. Rabani, D.W. Bahnemann, J.K. Dohrmann, J. Photochem. Photobiol. A 148 (2002) 169–176.
[45] A.R. Kortan, R. Hull, R.L. Opila, M.G. Bawendi, M.L. Steigerwald, P.J. Carroll, L.E. Brus, J. Am. Chem. Soc. 112 (1990) 1327–1332.
[46] N. Serpone, D. Lawless, R. Khairutdinov, E. Pelizzetti, J. Phys. Chem. 99 (1995) 16655–16661.
[47] G.P. Fotou, S.E. Pratsinis, Chem. Eng. Commun. 151 (1996) 251–269.
[48] T. Guo, Z. Bai, C. Wu, T. Zhu, Front. Environ. Sci. Eng. China 2 (2008) 224–229.
[49] P. Pichat, J.M. Hermann, in: N. Serpone, E. Pelizzetti (Eds.), Photocatalysis: Fundamentals and Applications, John Wiley & Sons, NTC, 1989, pp. 217–250.
[50] M.A. Fox, M.T. Dulay, Chem. Rev. 93 (1993) 341–357.
[51] S.B. Kim, H.T. Hwang, S.C. Hong, Chemosphere 48 (2002) 437–444.
[52] A.R. Gonzalez-Elipe, G. Munuera, J. Soria, J. Chem. Soc. Faraday Trans. I 75 (1979) 748–761.
[53] Y. Nakaoka, Y. Nosaka, J. Photochem. Photobiol. A 110 (1997) 299–305.
[54] R.I. Bickley, F.S. Stone, J. Catal. 31 (1973) 389–397.
[55] A.H. Boonstra, C.A.H.A. Mutsaers, J. Phys. Chem. 79 (1975) 1694–1698.
[56] N. Tian, Z.-Y. Zhou, S.-G. Sun, Y. Ding, Z.L. Wang, Science 316 (2007) 732–735.
[57] V. Komanicky, H. Iddir, K.-C. Chang, A. Menzel, G. Karapetrov, D.C. Hennessy, P. Zapol, H. You, Electrochim. Acta 55 (2010) 7934–7938.

[58] B. Roldan Cuenya, Thin Solid Films 518 (2010) 3127–3150.
[59] K. Chiang, R. Amal, T. Tran, J. Mol. Catal. A: Chem. 193 (2003) 285–297.
[60] C.H. Pollema, J.L. Hendrix, E.B. Milosavljevic, L. Solujic, J.H. Nelson, J. Photochem. Photobiol. A 66 (1992) 235–242.
[61] T.E. Jordan, Vapor Pressure of Organic Compounds, Interscience Publishers Inc., New York, 1954.
[62] H.G. Hirschenberg, Verfahrenstechnik und Anlagenblau: Chemie, Technik, Wirtschaftlichkeit, Springer, Berlin, 1999.